NUMERICAL ANALYSIS OF NATURAL CONVECTION IN OSCILLATING ENCLOSURES

Susie C. Keller – susie@cesup.ufrgs.br
Federal University of Rio Grande do Sul, Dep. of Pure and Applied Mathematics, PPGMAp
Av. Bento Gonçalves, 9500 – 90501-900 – Porto Alegre, RS, Brazil
Álvaro L. De Bortoli – dbortoli@mat.ufrgs.br
Federal University of Rio Grande do Sul, Dep. of Pure and Applied Mathematics,
Av. Bento Gonçalves, 9500 – 90501-900 – Porto Alegre, RS, Brazil

Abstract. *The present work develops a numerical method for the buoyancy–driven flow in rectangular enclosures. The configuration consists of two isolated horizontal walls and two vertical walls at temperatures T_{heat} and T_{cold}. The analysis is based on the incompressible formulation with the Boussinesq approximation, which is appropriate for relatively small temperature differences between the vertical walls. The method is based on the finite difference explicit Runge-Kutta multistage scheme for solving the Navier-Stokes, continuity and energy equations. Numerical tests are carried out for fixed and oscillating cavities, where the Coriolis force must be taken into consideration. Obtained results showed to compare well with numerical/experimental data found in the literature for steady and unsteady flow situations for Rayleigh numbers between 10^2 and 10^5 and Prandtl numbers ranging from 0.005 to 1.0.*

Keywords: ***N****atural convection, (Un)steady flows, Finite difference, Runge-Kutta.*

1. INTRODUCTION

In free convection the fluid flows naturally being driven by the effect of buoyancy, which is related to the tendency of gases to expand and to rise when heated, for example. It is know that this problem exhibits complex flow features depending on the Rayleigh number, cavity aspect ratio, temperature difference parameters and Prandtl number. For a heated vertical wall the fluid in the proximity of the plate tends to rise, while the fluid far enough from the plate remains undisturbed. Mass conservation requires that an equivalent quantity of mass go down at neighbourhood of the vertical plate.

The development of computational fluid dynamics and the advent of even more powerful computers allow the faster and more accurate calculation of flow fields inside configurations of technical interest. Cavities followed by fluids are components of a long list of engineering and geophysical systems (Bejan, 1984).

Common methods employed to solve natural convection flows are the finite volume, finite difference and finite elements. The finite difference is an easy and efficient one. Besides, for transient incompressible fluid flows it is better to employ explicit methods, because of the small pressure gradient. Therefore, the present work develops a finite

difference explicit Runge-Kutta multistage scheme, with central spatial discretization for the solution of mass conservation, Navier-Stokes (in *x* and *y* directions) and energy equation. Because of the advantages of the code structure it was possible to write an efficient numerical code.

Numerical tests are carried out for steady and unsteady flows for the Prandtl numbers between *0.005* to *1* and Rayleigh numbers between 10^2 and $6.5x10^5$, and they are found to compare well with numerical/experimental data found in the literature.

2. GOVERNING EQUATIONS

For relatively small temperature differences between the vertical walls the incompressible formulation with a Boussinesq approximation has shown to be appropriate for solving natural convection flows (Choi and Merkle, 1993; Maliska, 1995). So, momentum conservation equations are used to obtain velocity vector components, energy conservation to temperature and continuity equation for pressure. As pressure does not appear in an explicit form in the continuity equation, an equation for pressure is obtained through derivation of momentum equations in *x* and *y* directions, respectively, resulting a Poisson's equation, which takes into account the continuity relation. Although temperature differences originate velocity gradients, numerically the pressure-velocity coupling remains important. For bidimensional flows the set of governing equations can be written in the following form

Momentum conservation

x direction

$$\frac{\partial u}{\partial t} + u\frac{\partial u}{\partial x} + v\frac{\partial u}{\partial y} = -\frac{1}{\rho}\frac{\partial p}{\partial x} + \nu\left(\frac{\partial^2 u}{\partial x^2} + \frac{\partial^2 u}{\partial y^2}\right) \tag{1}$$

y direction

$$\frac{\partial v}{\partial t} + u\frac{\partial v}{\partial x} + v\frac{\partial v}{\partial y} = -\frac{1}{\rho}\frac{\partial p}{\partial y} + \nu\left(\frac{\partial^2 v}{\partial x^2} + \frac{\partial^2 v}{\partial y^2}\right) + g\beta\Delta T \tag{2}$$

Poisson's equation for pressure

$$\nabla^2 p = -\rho\left[\frac{\partial^2 (uu)}{\partial x^2} + 2\frac{\partial^2 (uv)}{\partial x \partial y} + \frac{\partial^2 (vv)}{\partial y^2}\right] - \rho\frac{\partial d}{\partial t} + \rho\nu\left[\frac{\partial^2 d}{\partial x^2} + \frac{\partial^2 d}{\partial y^2}\right] \tag{3}$$

Energy conservation

$$\frac{\partial T}{\partial t} + u\frac{\partial T}{\partial x} + v\frac{\partial T}{\partial y} = \alpha\left(\frac{\partial^2 T}{\partial x^2} + \frac{\partial^2 T}{\partial y^2}\right) \tag{4}$$

with $\alpha = \dfrac{K}{\rho c_p}$ and *d* is the continuity relation, $d = \dfrac{\partial u}{\partial x} + \dfrac{\partial v}{\partial y}$.

Here ρ is the fluid density , *u* and *v* the velocity vector components, *p* the pressure, *T* the temperature, *t* the time, ν the kinematic viscosity, *g* the acceleration of gravity, *K* the thermal conductivity, β the volumetric expansion coefficient, α the thermal difusivity and finally c_p the constant of specific heat transfer.

For oscillating cavities, on the other hand, the governing equations must be written taking into account the Coriolis forces, resulting the following set of equations

Momentum conservation

x direction

$$\frac{\partial u}{\partial t}+u\frac{\partial u}{\partial x}+v\frac{\partial u}{\partial y}-\left(2v\Omega+x\Omega^2+y\frac{d\Omega}{dt}\right)=-\frac{1}{\rho}\frac{\partial p}{\partial x}+\nu\left(\frac{\partial^2 u}{\partial x^2}+\frac{\partial^2 u}{\partial y^2}\right)+g\beta\Delta T(\sin\theta) \quad (5)$$

y direction

$$\frac{\partial v}{\partial t}+u\frac{\partial v}{\partial x}+v\frac{\partial v}{\partial y}+\left(2u\Omega-y\Omega^2+x\frac{d\Omega}{dt}\right)=-\frac{1}{\rho}\frac{\partial p}{\partial y}+\nu\left(\frac{\partial^2 v}{\partial x^2}+\frac{\partial^2 v}{\partial y^2}\right)+g\beta\Delta T(\cos\theta) \quad (6)$$

Poisson's pressure equation

$$\nabla^2 p=-\rho\left[\frac{\partial^2(uu)}{\partial x^2}+2\frac{\partial^2(uv)}{\partial x\partial y}+\frac{\partial^2(vv)}{\partial y^2}+\frac{\partial S_x}{\partial x}+\frac{\partial S_y}{\partial y}\right]-\rho\frac{\partial d}{\partial t}+\rho\nu\left[\frac{\partial^2 d}{\partial x^2}+\frac{\partial^2 d}{\partial y^2}\right] \quad (7)$$

where

$$S_x=g\beta\Delta T(\sin\theta)$$

$$S_y=g\beta\Delta T(\cos\theta)$$

with

$$\Omega=2\pi f\theta_{max}\cos(2\pi ft) \quad (8)$$

being θ the angle of inclination and θ_{max} it's maximum value, f the frequency of oscillation and Ω the angular velocity. Following the numerical procedure is indicated.

3. DESCRIPTION OF THE NUMERICAL METHOD

The set of governing equations (1) – (4) or (4) – (8) is approximated using the finite difference method because we intend to use a faster, accurate, simple and cheaper method. Joining the above factors central differences are used for convective as well as diffusive terms, while a forward approximation is adopted for time varrying terms based on Runge-Kutta time-stepping scheme.

The domain is divided into points, where each cell is labelled according to it's index point *(i,j)*, as show in Fig. 1 (Wendt, 1996). Both velocities, pressure and temperature are centred at each point *(i,j)*. Extension to generalised coordinates is based on the chain rule as well explained by Maliska (1995).

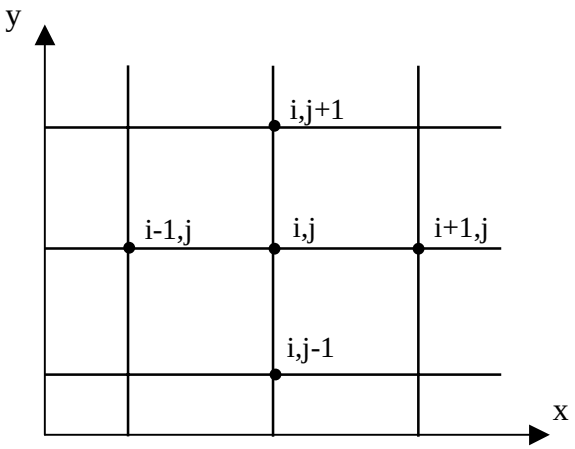

Figure 1 – Grid cell for each point (i,j) in the computational domain.

After approximation Eq. (5) results in the following form:
Momentum conservation
x direction

$$u_{ij} = u_{i,j}^{0} - \Delta t\left\{u_{i,j}\left(\frac{u_{i+1,j} - u_{i-1,j}}{2\Delta x}\right) + v_{i,j}\left(\frac{u_{i,j+1} - u_{i,j-1}}{2\Delta y}\right) - \left(2v_{i,j}\Omega + x_{i,j}\Omega^{2} + y_{i,j}\left(\frac{\Omega - \Omega^{0}}{\Delta t}\right)\right)\right.$$
$$\left. + \frac{p_{i+1,j} - p_{i-1,j}}{2\Delta x} - \nu\left[\frac{u_{i+1,j} - 2u_{i,j} + u_{i-1,j}}{\Delta x^{2}} + \frac{u_{i,j+1} - 2u_{i,j} + u_{i,j-1}}{\Delta y^{2}}\right] - g\beta\left(T_{i,j}^{0} - To\right)\sin(\theta)\right\} \quad (9)$$

The other equations, momentum in *y* direction, Poisson and energy, are approximated in a similar manner.

Wall boundary conditions are no slip, two isolated horizontal walls and two vertical walls at different temperatures and zero normal pressure gradient. In reality the pressure must be fixed at least at one point, because pressure gradients are necessary in order to originate velocity gradients. Besides, pressure values are approximatly the atmospheric value.

4. NUMERICAL RESULTS

In the following, numerical results for rectangular cavities are presented and compared with numerical/experimental data found in the literature. Streamlines and isothermals are employed because they well represent the problem of interest. The results are divided in two classes: for steady and unsteady flows.

4.1. Results for steady flows

The first case considers the flow into a square closed cavity *(1 x 1)*, heated at its left side and cooled at right side, being the horizontal walls isolated. In all cases the basic form of the flowfield is a recirculatting roll. This recirculation is driven by the generation of vorticity by the horizontal temperature gradient of *100* degrees (*313K - 213K*) for Prandtl *0.733* (used for gases). The computational mesh used contains *30 x 30* cells and a stretching factor *1.05* from cell to cell in both *x* and *y* directions, obtaining adequate concentration mainly at proximity of corners.

Figure 2 and 3 show the streamlines for varying Rayleigh numbers between 10^2 and 10^5, whose agreement with the results found by Arpace and Larsen (1984) is adequate. Although the streamline values were not indicated, their behaviors is similar and were obtained by different numerical methods.

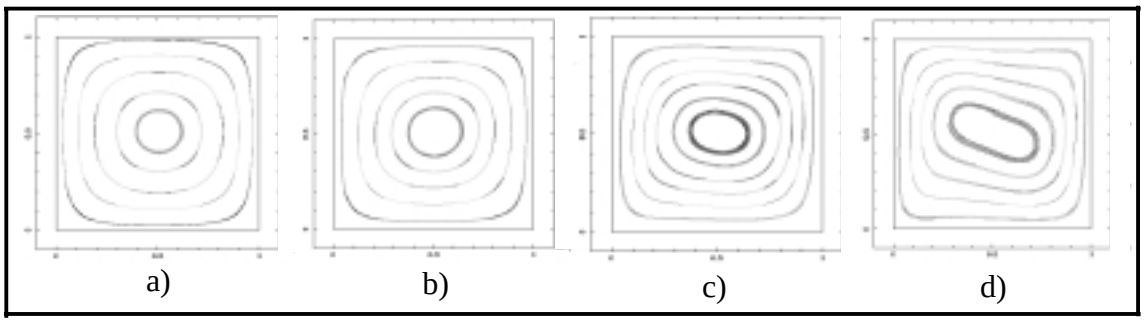

Figure 2 - Streamlines for square cavity for Rayleigh a)10^2, b)$2.5x10^3$, c)$2.5x10^4$ and d)10^5.

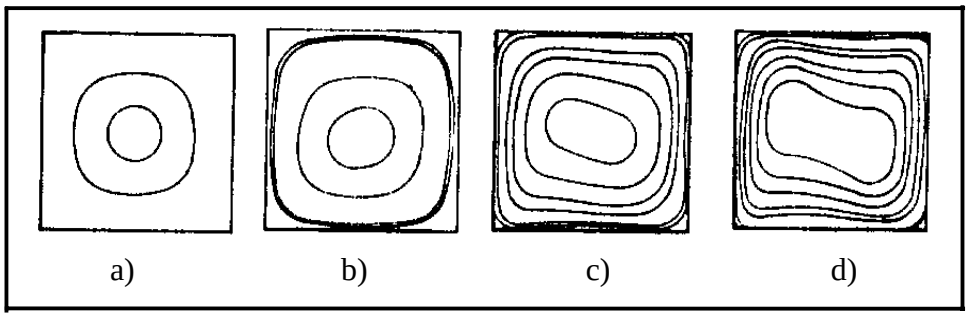

Figure 3 - Streamlines for square cavity from Arpace and Larsen (1984) for Rayleigh a)10^2, b)$2.5x10^3$, c)$2.5x10^4$ and d)10^5.

The isothermals have the same behavior as shown in Fig. 4 and 5. For Rayleigh 10^2 heat propagates from the walls until the cavity center, because at this Rayleigh number the diffusion is dominant for $Pr = 0.733$ ($Pr < 1$). So, the viscous effects scatter almost in a linear way, originating a circular movement inside the cavity (Maliska, 1995).

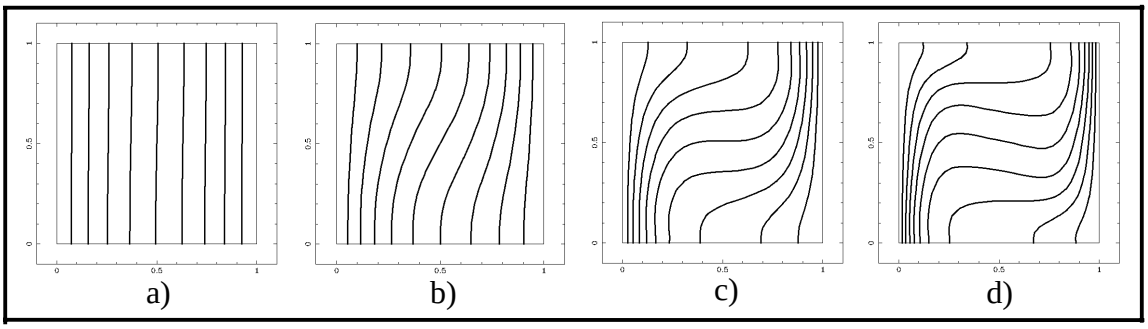

Figure 4 – Isothermals for square cavity for Rayleigh a)10^2, b)$2.5x10^3$, c)$2.5x10^4$ and d)10^5.

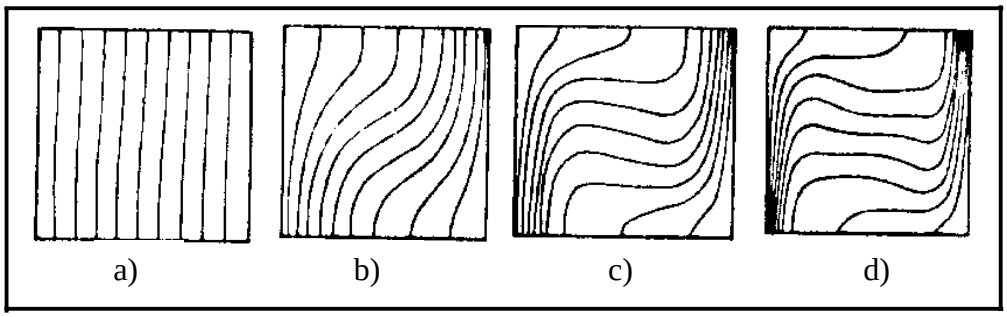

Figure 5 - Isothermals for square cavity as Arpace and Larsen (1984) for Rayleigh a)10^2, b)$2.5x10^3$, c)$2.5x10^4$ and d)10^5.

Increasing the Rayleigh number to $2.5x10^3$ the isothermals start to be more curved. The same behavior is also observed for $Ra = 10^5$, but now the temperature effects not propagate until the cavity center as before (iso temperature lines remain almost horizontal at cavity center).

Now a rectangular *1 x 4* cavity and a grid containing *40 x 60* uniform distributed points is used. Grid stretching turns the convergence of the finite difference method more difficult, specially when the stretching factor is bigger them *1.2* (or *20%* increase from cell to cell). Figure 6 and 7 show the streamlines for rectangular *1 x 4* cavity for Rayleigh between 10^2 and

2.2x10^3 for different Prandtl numbers (between *0.005* and *1*). Prandtl of order *1* is common for gases. An adequate resemblance between our and the literature results is observed. Remember that the number of curves is not the same, because their values were not indicated in the literature (Alchaar and Vasseur, 1995).

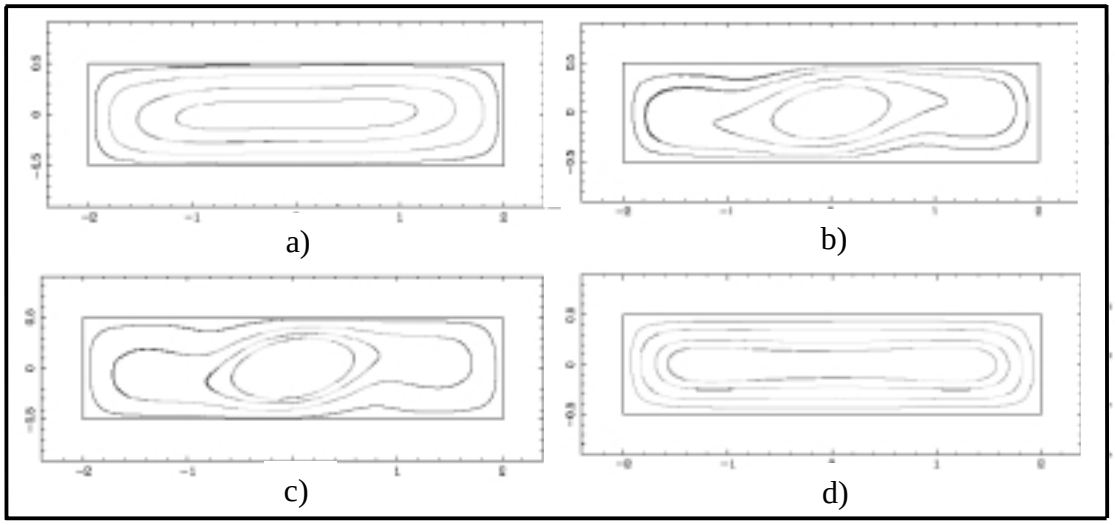

Figure 6 - Streamlines for 1x4 rectangular cavity a)Ra=2x10^2 and Pr=0.01, b)Ra=8x10^2 and Pr=0.01,c)Ra=4x10^2 and Pr=0.005 and d)Ra=2.2x10^3 and Pr=1.

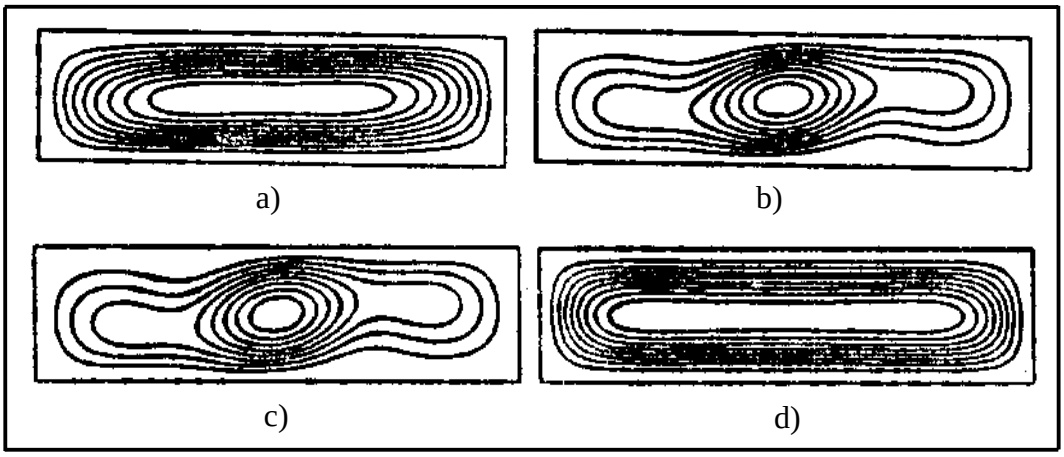

Figure 7 - Streamlines for 1x4 rectangular cavity as Alchaar and Vasseur (1995), a)Ra=2x10^2 and Pr=0.01, b)Ra=8x10^2 and Pr=0.01, c)Ra=4x10^2 and Pr=0.005 and d)Ra=2.2x10^3 and Pr=1.

Following, numerical results for small curved enclosures are presented in order to identify if important differences for the same Rayleigh and Prandtl numbers appear. Figure 8 shows the streamlines for curved *1 x 4* cavity for internal *2,05* and external *3,05* radios, respectively. Again, the fluid flows parallel to the upper and lower surfaces and near the corners it rotates *180°* degrees. Although Rayleigh is equal to *10*^{2} in Figs. 8a) and 9a), the convective effects are stronger because of the small Prandtl number. For Rayleigh 8*x10*^{2} and Prandtl *0.01* the parallel flow structure starts to broken. For Prandtl *1* and Rayleigh *2.2x10*^{3} the flow recuperates its initial configuration, which means that appear a recirculating big vortex inside the complete cavity. More interestingly results can be obtained increasing again

Rayleigh number for small Prandtl numbers. However, such transient and turbulent flow behavior is very complex and will be analysed in a future work.

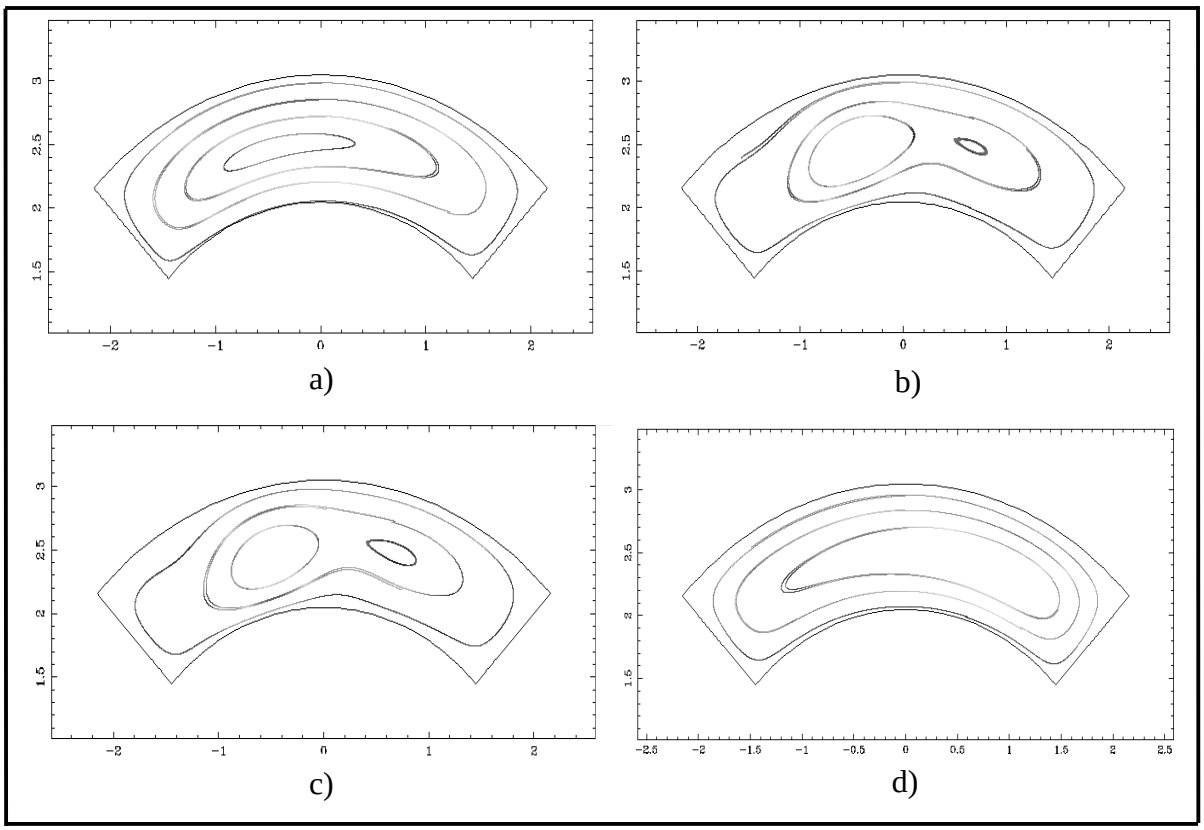

Figure 8 – Streamlines for rectangular 1 x 4 curved cavity a)Ra=$2x10^2$, Pr=0.01; b)Ra=$8x10^2$, Pr=0.01; c)Ra=$4x10^2$, Pr=0.005 and d)Ra=$2.2x10^3$, Pr=1.

4.2 Unsteady cavity flows

After calibration of the numerical code for steady flows, considers the transient flow inside a square closed *1 x 1* cavity, with its left side at *213K* and the right side at *363K*, being the two horizontal walls isolated. Considers that the enclosure oscillates around its center axis. In this way, at a special time with $\theta = 0$ the flutuability effects will accelerate the flow to follow in a certain way, while the Coriolis forces will act on the opposite side, depending on the instantaneous direction of cavity acceleration.

For this flow situation small recirculations appear and the grid needs to be refined. So a *90 x 90* mesh was employed for a stretching factor *1.02* through the use of an in-house mesh generator (simple and efficient one). Obtained results from Moh et al. (1996) were used for comparison, although they employed more complex numerical techniques. First results were obtained for $Pr = 0.02$ and $Ra = 1.2x10^5$ for the fundamental frequency of oscillation $f = 329.6$ (For details see Moh et al., 1996). The cavity oscillates between *10* and *–10* degrees.

Figure 9 and 10 display the isothermals obtained for this flow situation for times varying between $t = 0.5006$ and $t = 0.5034$, and show that they are concentrated at proximity of vertical walls.

Following, numerical results for $Pr = 0.03$ and $Ra = 6.5x10^5$ for frequency $f = 829.88$ are also presented. Here a central vortex appear together with four small vortices at proximity of cavity corners, as well as other small vortices at proximity of cavity center.

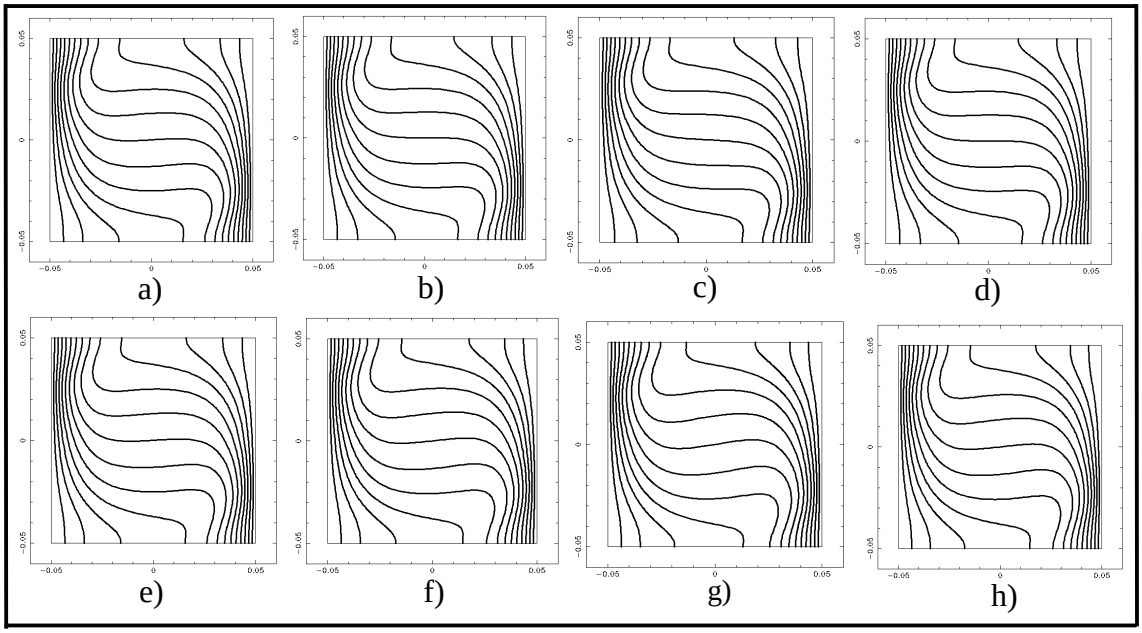

Figure 9 - Isothermals for square cavity at special time and angles for Rayleigh $1.2x10^5$ a)t=0.5006, θ=0°; b)t=0.5009, θ=5°; c)t=0.5014, θ=10°; d)t=0.5019, θ=5°; e)t=0.5021, θ=0°; f)t=0.5024, θ=-5°; g)t=0.50029, θ=-10° and h)t=0.5034, θ=-5°.

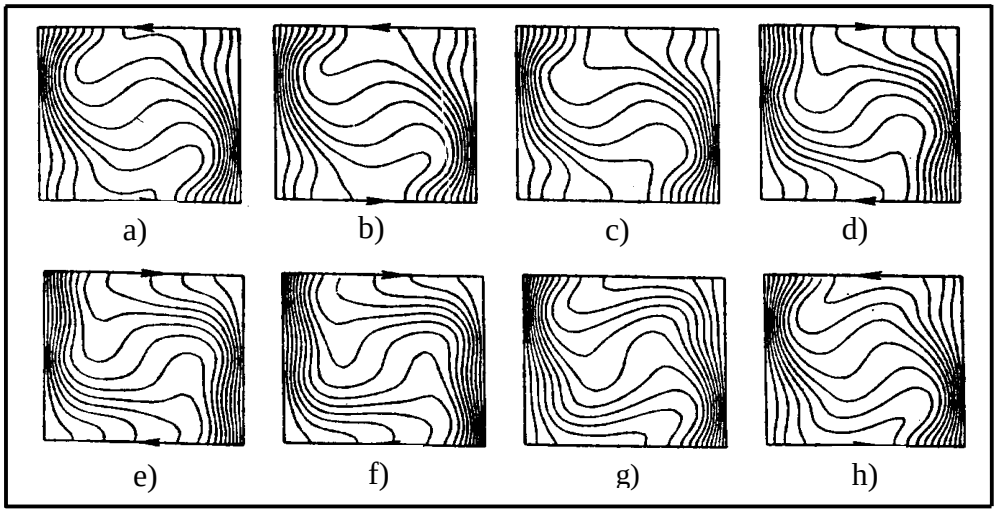

Figure 10 - Isothermals for square cavity at special time and angles for Rayleigh $1.2x10^5$ as Moh et al (1996) a)t=0.5006, θ=0°; b)t=0.5009, θ=5°; c)t=0.5014, θ=10°; d)t=0.5019, θ=5°; e)t=0.5021, θ=0°; f)t=0.5024, θ=-5°; g)t=0.50029, θ=-10° and h)t=0.5034, θ=-5°.

These secondary rolls are generated because at high Rayleigh and/or small Prandtl numbers there is an intense development of thermal boundary layers in the vicinity of the wall, which leads to sign reversal for the temperature and pressure gradients (Choi and Merkle, 1993).

General behavior obtained through comparison of Figs. 11 and 12 is the same except for Fig. (12c)). Such a behavior seems to be not real, besides the vortices at corners almost disappeared, what can be related to deficiencies of the numerical technique employed or the postprocessing software used by Moh et al (1996).

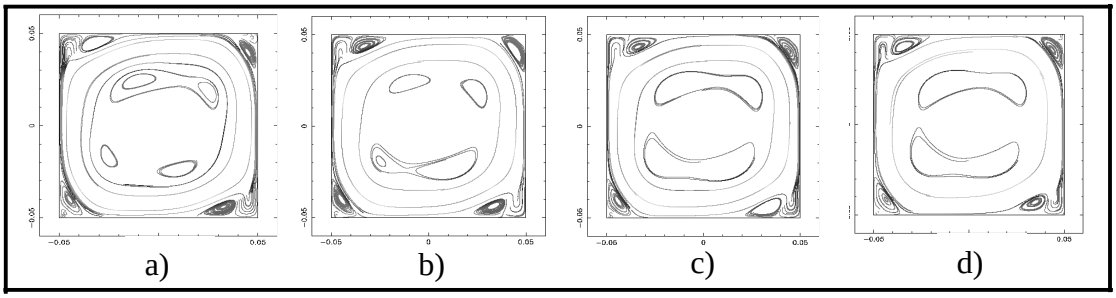

Figure 11 – Streamlines for unsteady flow in a 1 x 1 square cavity a)t=0.5, b)t=0.5004, c)t=0.5007 and d)t=0.501.

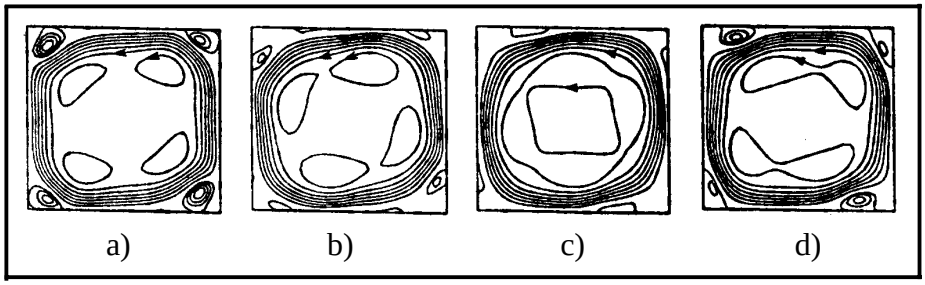

Figure 12 – Streamlines for unsteady flow in a 1 x 1 square cavity as Moh et al (1996) a)t=0.5, b)t=0.5004, c)t=0.5007 and d)t=0.501.

Finally, Fig. 13 and 14 show the isothermals for the same flow situation as shown by Figs. 11 and 12. It can be said that the agreement between the results indicated by both figures is adequate. Isothermals are concentrated in the neighborhood of vertical walls, as expected, because of the high Rayleigh and small Prandtl numbers.

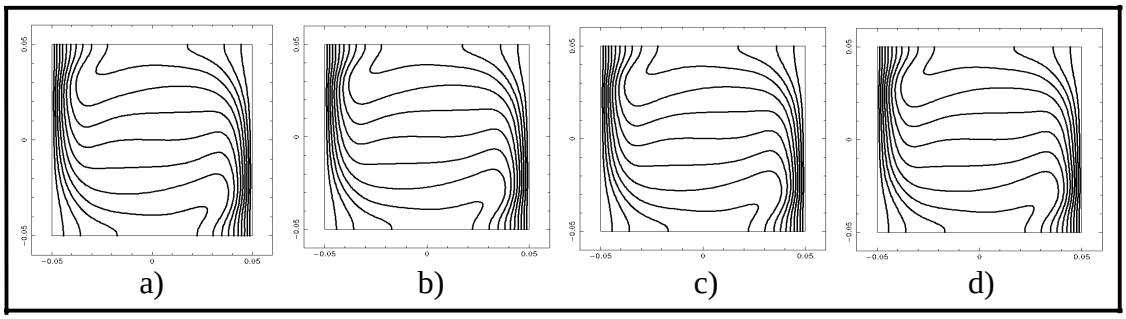

Figure 13 – Isothermals for unsteady flow in a 1 x 1 square cavity, a)t=0.5, b)t=0.5004, c)t=0.5007 and d)t=0.501.

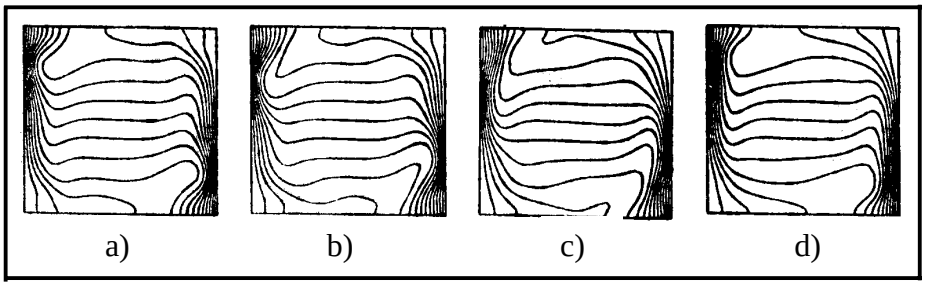

Figure 14 – Isothermals for unsteady flow in a 1 x 1 square cavity as Moh et al (1996) a)t=0.5, b)t=0.5004, c)t=0.5007 and d)t=0.501.

5. CONCLUSIONS

Numerical results show that the method used here is able to well represent steady and unsteady flows inside cavities. Big and small recirculation zones were well represented when compared with numerical results found in the literature employing more complex and, consequently, more expensive numerical methods.

Tests using CRAY T94 showed a code performance of around 1040 Mflops, what means that the code was efficiently written. Remember that commercial codes used at same computer have performance usually less than 200 Mflops.

Special care has been taken at treatment of Coriolis terms when solving flows for rotating cavities. Besides, for curved geometries a generalized form of governing equations was necessary in order to represent the flow behavior.

It was shown that the counter-rotating simple vortex configuration appears for square and rectangular cavities. For rectangular cavities of 1x4 and 1x10 and for high Rayleigh and low Prandtl numbers the counter rotating double vortex starts to appear. Besides, increasing Prandtl number decrease the flow instabilities, as expected.

Several additional problems have also been successfully computed with this method but are not presented here for reasons of space. As it can be seen, this work opens several possibilities for natural convection application analysis, mainly because of its characteristics in generalized coordinates. Performance of the developed code showed to be the same when solving flows into curved cavities.

Therefore, the author's opinion is that the numerical results are encouraging. However, much work must still be done in order to obtain unsteady flows into cavities for smaller Prandtl and higher Rayleigh numbers that the ones presented in this work.

6. ACKNOWLEDGEMENT

Computations were performed at the computer CRAY T94 of CESUP – UFRGS. The support and assistance of the staff is gratefully acknowledged.

7. REFERENCES

Alchaar, S., Vasseur, P., 1995, Natural Convection Heat Transfer in a Rectangular Enclosure with a Transverse Magnetic Field, Journal of Heat Transfer, vol. 117, pp. 668-673.

Arpace, V. S., Larsen P.S., 1994, Convection Heat Transfer, Prentice-Hall Inc., Englewood Cliffs.

Bejan, A., 1984, Convection Heat Transfer, John Wiley & Sons, Inc., New York.

Choi, Y. H., Merkle, C. L., 1993, The Application of Preconditioning in Viscous Flows, Journal of Computational Physics, vol. 105, pp. 207-223.

Maliska, C. R., 1995, Transferência de Calor e Mecânica dos Fluidos Computacional, Editora Livro Técnico e Científico, Rio de Janeiro.

Moh, J.H., Bergman, T.L., Kuv, D.C., 1996, Simulation of Two-Dimensional Low-Pr Natural Convection in Harmonically Oscillated, Differentially Heated Enclosure, Numerical Heat Transfer, Part A, vol. 31, pp. 1-19.

Wendt, J. H., 1996, Computational Fluid Dynamics, Springer-Verlag, Berlin.